Quaternary Research (2024), **122**, 62–75
doi:10.1017/qua.2024.17

Research Article

Insights into the synergistic effects of tectonics and climate from the formation and evolution of the Hongwen allochthonous deposit, southwestern China

Yuchao Li[a], Jianping Chen[a], Qing Wang[a]*, Zhihai Li[b], Yansong Zhang[a] and Jianhua Yan[c]

[a]College of Construction Engineering, Jilin University, Changchun, Jilin 130026, China; [b]Zhejiang Huadong Construction Corporation Limited, POWERCHINA Huadong Engineering Corporation Limited, 310014, Hangzhou, Zhejiang, China and [c]College of Earth Sciences and Engineering, Hohai University, Nanjing 210098, China

Abstract

The formation and evolution of large-scale deposits generated by mass movement are often closely related to tectonic and climatic conditions. Investigating deposits under the influence of complex geological conditions can aid in reconstructing paleoenvironmental characteristics and fluvial geomorphic evolution. The First Bend of the Yangtze River (FBYR), located in the Jinsha River basin in southwest China, represents a significant section characterized by abundant allochthonous deposits. We conducted a detailed investigation of the Hongwen allochthonous deposit (HAD) and the river sediments in the First Bend. Through terrain interpretation, dating, and paleoenvironmental analysis, the HAD was determined to be a complex deposit with multiple sources and stages (46.4–33.5 ka), formed under the combined influence of tectonic activity and climate. Three mass-movement events occurred during the interglacial stage of the last glacial period or its transitional period, coinciding with the rapid uplift stage of the Tibetan Plateau since the late Pleistocene. Prominent features of this period include significant rainfall and tectonic activities. By dating fluvial sediments and examining the evolution of the HAD, we revealed a river incision rate of 2.30 mm/yr for the Jinsha River, providing a basis for analyzing periodic river cutting and the development pattern of surface processes.

Keywords: Allochthonous deposit, Genetic mechanism, Dating, Paleoclimate and paleostructure, Evolution of fluvial geomorphology

Introduction

The Tibetan Plateau is the most structurally active area in the world (Lai et al., 2022), where many large rivers develop (Zhan et al., 2018). Influenced by collision of the Indian and Eurasian plates (Zhang et al., 2000; Li et al., 2015), the Tibetan Plateau and its surrounding areas have been uplifting rapidly since the middle to late Pleistocene (Li et al., 2020), which was accompanied by several glacial periods (Shi et al., 1999, 2001). Consequently, deposits are extensively distributed on both sides of the river valleys due to the combined effects of tectonic uplift, river incision, and climate change. The formation and evolution of deposits have been widely recognized as crucial aspects in understanding geological history (Zhan et al., 2018; Li et al., 2020). Research indicates that the Quaternary allochthonous deposits in the southeastern margin of the Qinghai–Tibet Plateau are primarily attributed to surface processes such as debris flows, landslides, or rock collapses (Korup and Montomery, 2008; Wu et al., 2016). Under natural conditions, deposits are often difficult to preserve in a well-maintained state due to the influence of dynamic surface processes (Li et al., 2020). However, certain factors such as terrain, scale, and material composition play significant roles in the long-term preservation of some deposits (Fan et al., 2020).

The interaction between geological structure and climate is recognized as the primary factor influencing surface processes (Li et al., 2022a). Consequently, the focal points and challenges of paleo-deposit research revolve around comprehending paleoenvironmental characteristics, elucidating genetic mechanisms, and analyzing the patterns of formation and evolution (Trauth and Strecker, 1999; Korup and Clague, 2009; Wang et al., 2014; Bao et al., 2020; Li et al., 2022b). Field investigation and chronological research serve as the foundation for addressing these issues. Field investigation allows for the effective collection of geological characteristics of deposits, enabling preliminary assessments of deposit types and causes (Costa and Schuster, 1988; Strom, 2004; Dunning, 2006; Chen et al., 2013). Chronological dating has made significant advancements through the development of luminescence and cosmogenic nuclide techniques (Hermanns et al., 2004; Chen et al., 2018). These advancements have greatly enhanced our ability to analyze the structural and climatic background of paleo deposits. Additionally, progress in science and computer technology has facilitated research in various fields such as geophysics, geochemistry, and numerical simulation. These disciplines have further contributed to the understanding of paleoenvironments related to deposits, causal mechanisms, and geomorphological evolution (Kong et al., 2009; Yan et al., 2022; Y.S. Zhang et al., 2022).

The Shigu section of the Jinsha River (the First Bend of the Yangtze River–FBYR), located in Hengduan Mountains belt

*Corresponding author email address: wangqing@jlu.edu.cn

Cite this article: Li Y, Chen J, Wang Q, Li Z, Zhang Y, Yan J (2024). Insights into the synergistic effects of tectonics and climate from the formation and evolution of the Hongwen allochthonous deposit, southwestern China. *Quaternary Research* **122**, 62–75. https://doi.org/10.1017/qua.2024.17

(Fig. 1a), has gained considerable attention due to its unique geomorphological feature known as the "First Bend" (Kong et al., 2012; Li et al., 2022b). In this study, we focus on the Hongwen allochthonous deposit (HAD) within the FBYR as a crucial window to understand the regional history of the geological environment. We delve into the formation and evolution mechanisms of the HAD through terrain interpretation, dating techniques, and paleoenvironmental analysis. Furthermore, we discuss the intertwined influences of tectonic activity and climate on the deposit. By integrating these insights with the developmental features of fluvial sediments in the FBYR, a sequence of river landform evolution is proposed.

Geological Setting

Regional tectonics and stratigraphy

The southeastern margin of the Tibetan Plateau has exhibited intense tectonic activity since the Cenozoic, with the Three-River belt and the Ailaoshan–Red River shear zone serving as representative regions in this context (Burchfiel and Chen, 2012). These fault zones, along with other large faults, establish the fundamental structural framework of the study area (Fig. 1b). The Ailaoshan–Red River shear zone commenced ductile left-slip movement at circa 27–17 Ma (Searle et al., 2010; Wei et al., 2016). However, in the Quaternary, three important NE-trending left-lateral faults (Lijiang, Heqing, and Jianchuan faults; Allen et al., 1984) were derived from the shear zone under the influence of brittle right-lateral faulting (Allen et al., 1984) (Fig. 2a). These faults exhibit left-lateral shearing, which can be attributed to either right-lateral movement along the Ailaoshan–Red River shear zone or subduction of the Indian plate beneath the Eurasian plate (Tapponnier et al., 1986; Wang and Burchfiel, 2000). In addition, the internal dynamic geological processes generated by large faults such as Jinshajiang and Xianshuihe also have a significant effect on the regional geological evolution. Alkali magmatism occurred in western Yunnan during the late Eocene to Oligocene, which is effective evidence of active crust and lithospheric extension (Chung et al., 1997).

The study area exhibits a well-developed stratigraphy. Dividing the area along the Shigu and Yangbi valleys, the western side is dominated by Cenozoic and Paleozoic strata, whereas the eastern side consists of Mesozoic and Paleozoic strata (Fig. 2a). The exposed strata in the First Bend primarily are pre-Triassic marine sedimentary strata (Fig. 2b). The predominant lithologies include limestone, slate, and schist. Additionally, the valley is characterized by widespread distribution of fluvial sediments, primarily of Cenozoic age.

Plateau uplift and climate background

Plateau uplift, which is the most important driving force of geomorphic evolution in southeastern Tibet, has been hotly debated over the past few years (Li et al., 2015; Zhan et al., 2018). A credible view is that uplift of the Tibetan Plateau is caused by the continuous thickening of the lithosphere due to the subduction of the Indian plate under the Eurasian plate (Li et al., 2015; Y.S. Zhang et al., 2022). Although the geological evolution of the plateau continues, the recognition that it uplifted rapidly in the Quaternary is widely accepted (Li et al., 2015). The average uplift rate of the Tibetan Plateau after the Early Pleistocene was 1.60–5.35 mm/yr, and the uplift rate of some areas exceeded 10 mm/yr in the Holocene (Fig. 3a) (Xiao and Wang, 1998). According to precision-leveling data of the surrounding area from 1970 to 2012 (Hao et al., 2014; Zhan et al., 2018), the annual average uplift rate of the First Bend section and the Yangbi valley is determined to be less than 3 mm/yr (Fig. 3b).

The uplift history of the Tibetan Plateau has a profound effect on the development and evolution of Quaternary glaciers. The coupling of mountain uplift and global glacial climate is the fundamental reason for the development of glaciers in the Tibetan Plateau and its surrounding mountain areas (Fig. 4a). The Kunhuang Movement that occurred during 1.1–0.6 Ma was characterized by a large-scale regional uplift in the early stage. In the later stage, there was primarily sudden uplift or subsidence of fault blocks, from which the Tibetan Plateau rose to more than 3000 m and developed the largest glaciation—the Kunlun

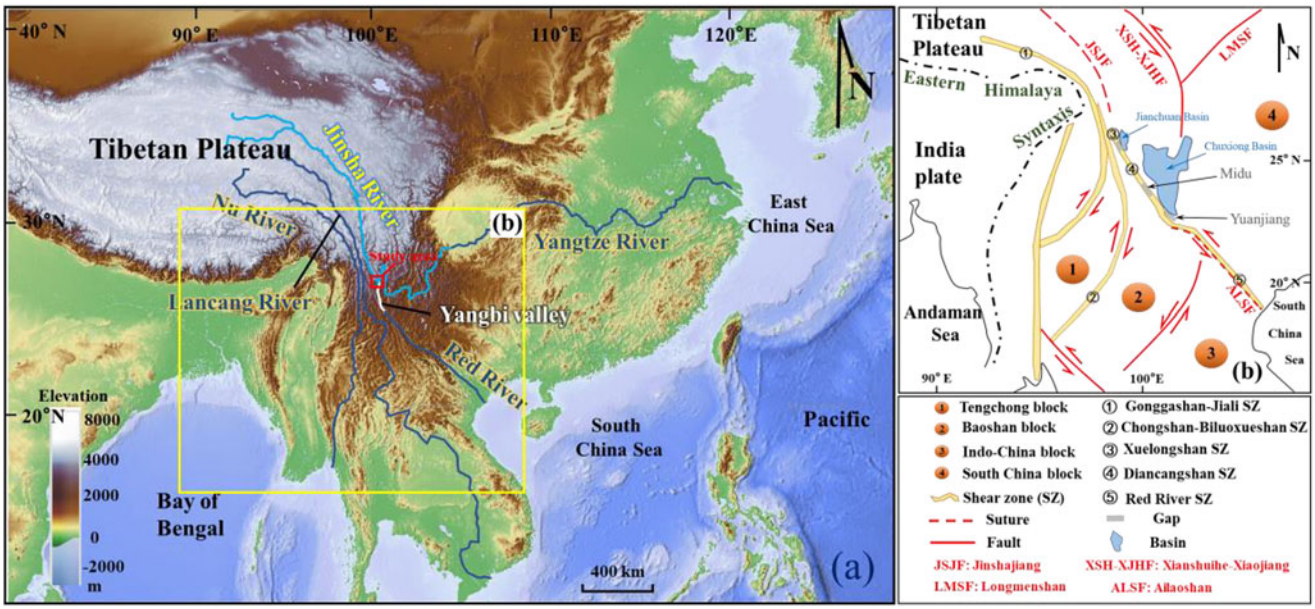

Figure 1. (a) Digital elevation model map showing major rivers of Southeast Asia. (b) Tectonic framework of southeastern Tibetan Plateau.

https://doi.org/10.1017/qua.2024.17 Published online by Cambridge University Press

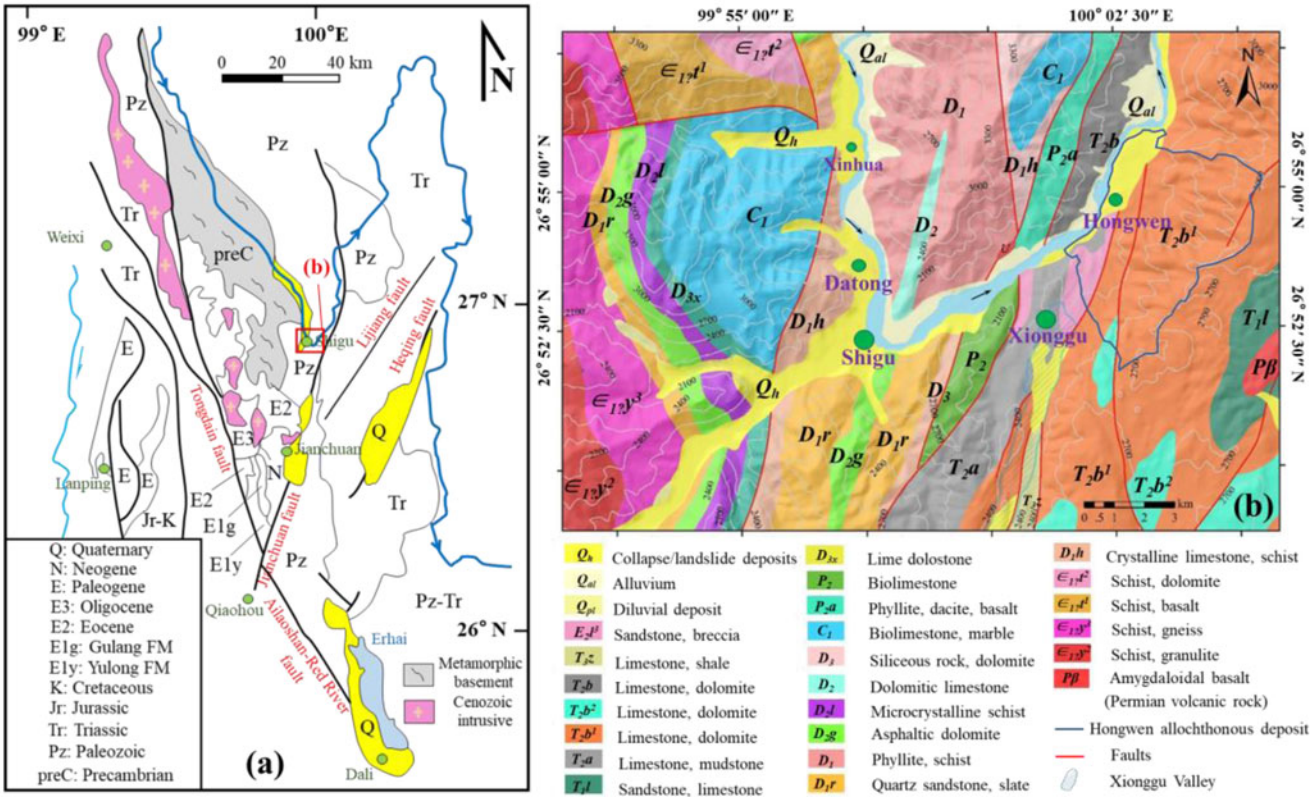

Figure 2. (a) Simplified geological map of southeastern Tibetan Plateau showing main faults, distributions of strata and intrusions, and the course of the Jinsha River (revised from Wei et al., 2016); location of Figure 2b shown with red box. (b) Geological map of the First Bend of the Yangtze River (FBYR).

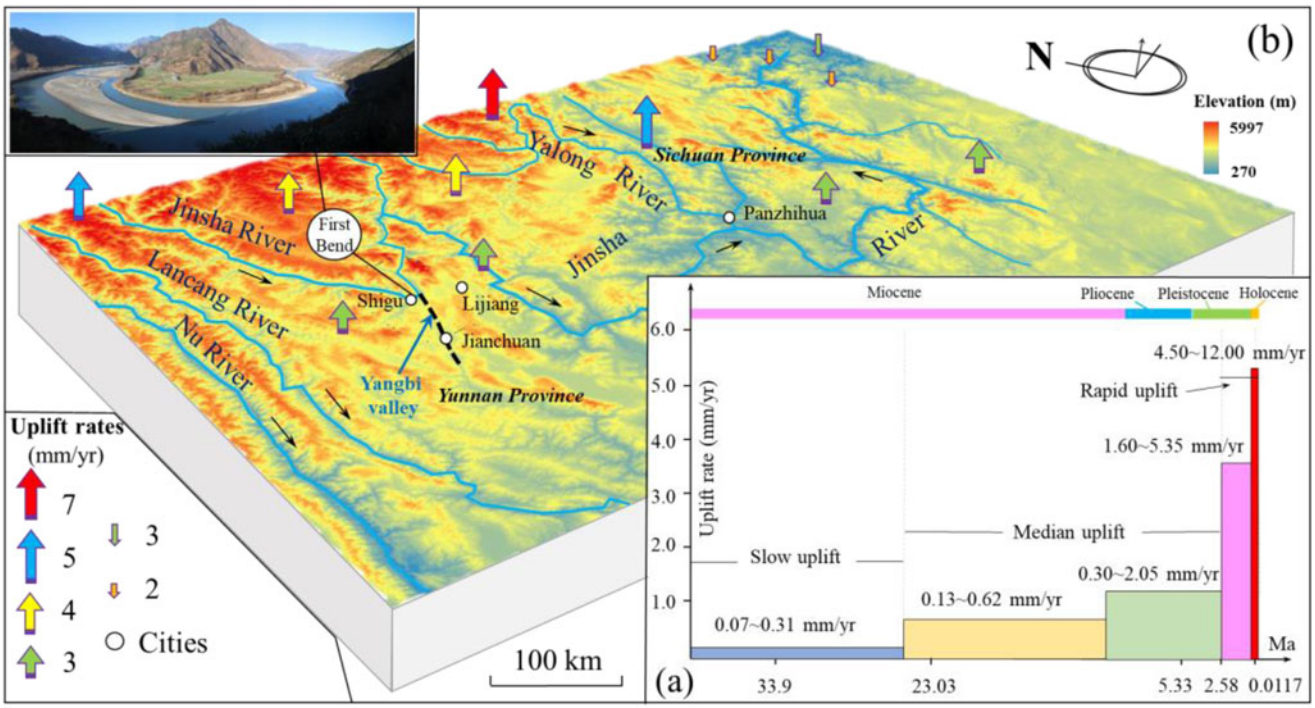

Figure 3. (a) Uplift rates of the Qinghai Tibet Plateau, revised from Zhan et al. (2018). (b) Vertical uplift velocity in northwest Yunnan with respect to the Sichuan basin (referenced from Hao et al., 2014); inset shows photographic image of the FBYR.

https://doi.org/10.1017/qua.2024.17 Published online by Cambridge University Press

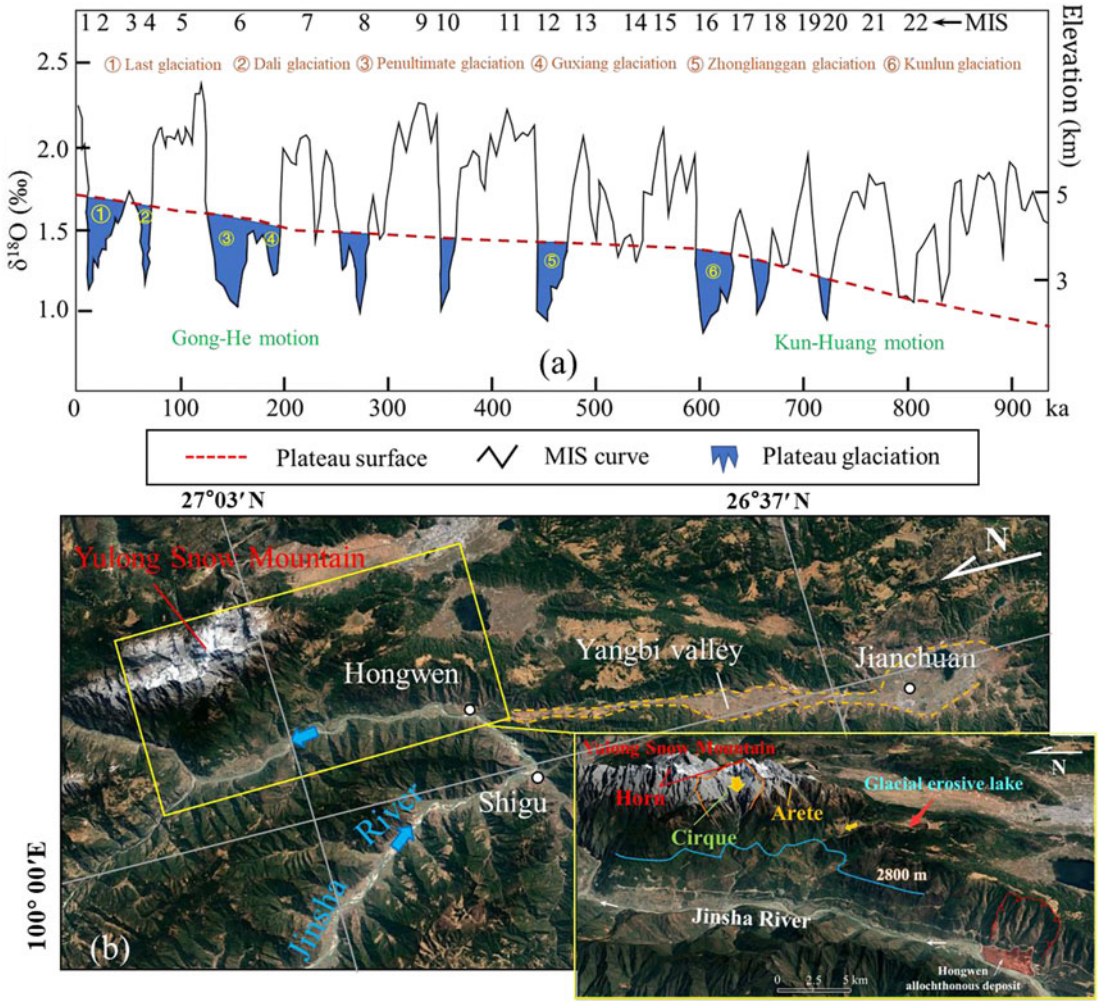

Figure 4. (a) Schematic diagram of the coupling between uplift of the Qinghai-Tibet Plateau and the Quaternary glaciation, revised from Zhou et al. (2006). (b) Characteristics of glacier development in Yulong Snow Mountain region.

glaciation (MIS 16) (Cui et al., 1998). About 0.15 Ma ago, under the influence of the Gonghe Movement (Li et al., 1996), many mountains on the southeastern margin of the Tibetan Plateau were uplifted above the glacial equilibrium line, and the penultimate (MIS 6) and last (MIS 4–2) glaciations occurred successively. The glacial and interglacial cycles represent the alternation of cold and warm (EPICA community members, 2004). Under the action of glacial freezing–thawing and scouring, the Yulong Snow Mountain area, situated in the lower reaches of the study area, witnessed the development of extensive moraines. The activity range of these moraines extended up to an elevation of nearly 2800 m (Fig. 4b).

Quaternary allochthonous deposit

The topography of the study area is undulating (Fig. 5a) due to regional uplift, river incision, and glacial activity. Quaternary allochthonous deposits are prevalent in the area (Fig. 5b). Considering the widespread existence of small-scale deposits and the limited accuracy of remote-sensing interpretations, only large-scale mass movements are listed in this study. Referring to the classification of movement types (Hungr et al., 2014), allochthonous deposits are simplified as landslide (6), debris flow (13), and bedrock deformation body (6). All deposits were confirmed by field survey and remote-sensing interpretation. 3D imagery was analyzed to determine the location and dimensions of the deposits (Fig. 5b). The HAD, located at the junction of the Jinsha and the Yangbi valley, with an average length of 4 km and average width of 1–1.5 km, is a multi-source, multi-stage, and complex deposit (Fig. 5c). The HAD is an excellent window to understand the paleoenvironment and geomorphic evolution, due to its long history, complex geological features, and special geographical location.

Methodology

Field observations

The geological characteristics of the HAD and the traceability of river sediments were the primary foci of the field investigation, providing essential foundations for the analysis of geomorphological evolution. Based on morphological and sedimentological characteristics, the HAD is divided into three distinct parts (Fig. 6a): Part I (3.52 km^2), Part II (0.53 km^2), and Part III (0.97 km^2) (Fig. 6b). The valleys located on the eastern side of these parts serve as the source areas (Fig. 6c). In order to obtain more specific geological characteristics of the allochthonous deposit and the river sediment, a detailed survey of representative outcrops was conducted in each part. Additionally, we traced the development of river terraces upstream of the deposit.

https://doi.org/10.1017/qua.2024.17 Published online by Cambridge University Press

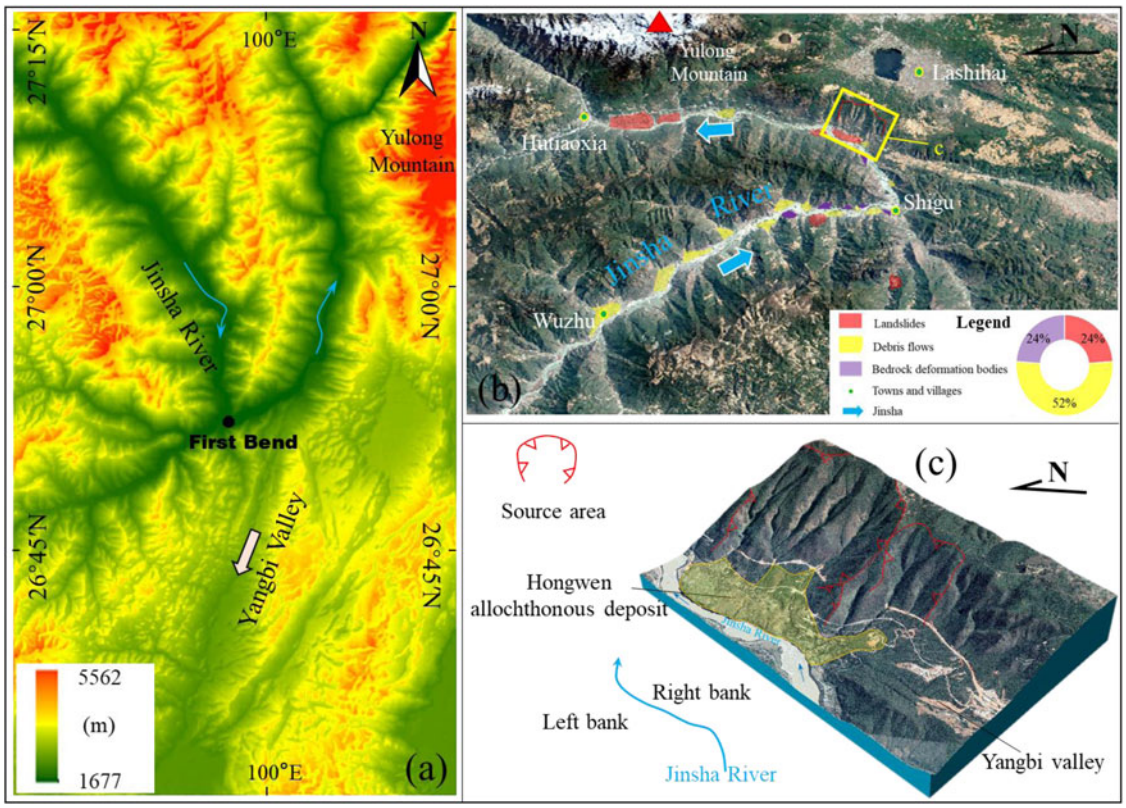

Figure 5. (a) Topographic characteristics of the FBYR. (b) Distribution of allochthonous deposits in the FBYR; yellow rectangle indicates location of Figure 5c. (c) Hongwen allochthonous deposit (HAD).

Sampling and dating

Chronology of the HAD and river sediments is of great significance for analysis of the genetic mechanism of the HAD and the evolution of fluvial geomorphology. Thermoluminescence (TL) is a process in which substances that have previously absorbed radiant energy release photons under excitation by heat. In sediments, the annual radiation dose received by crystalline material

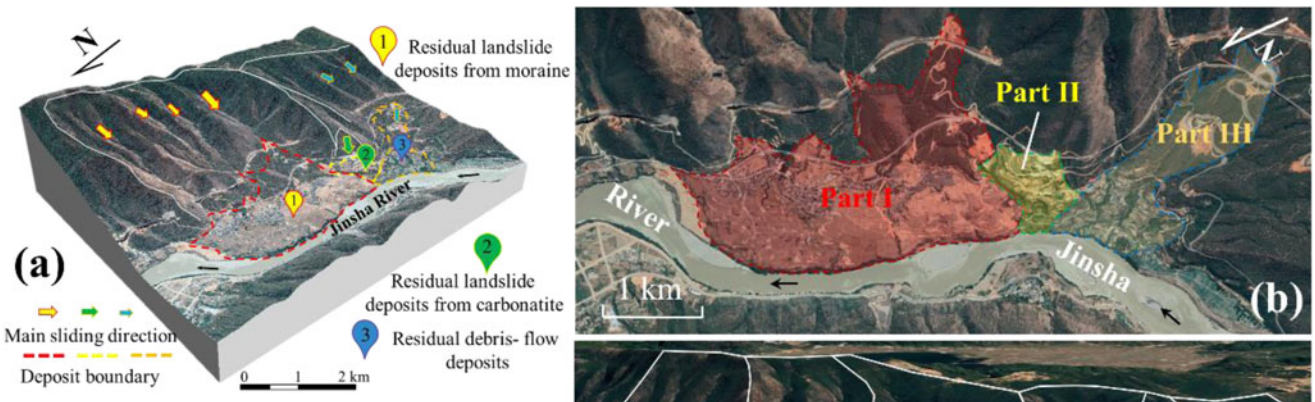

Part	Types of deposits	Material source	Area (km²)
I	Landslide	Moraine	3.52
II	Landslide	Rock slope	0.53
III	Debris-flow	Overburden	0.97

Figure 6. (a) Characteristics of zoning in the HAD. (b) Geometric features of the different parts in the HAD. (c) Topographic features of the source areas of the different parts.

https://doi.org/10.1017/qua.2024.17 Published online by Cambridge University Press

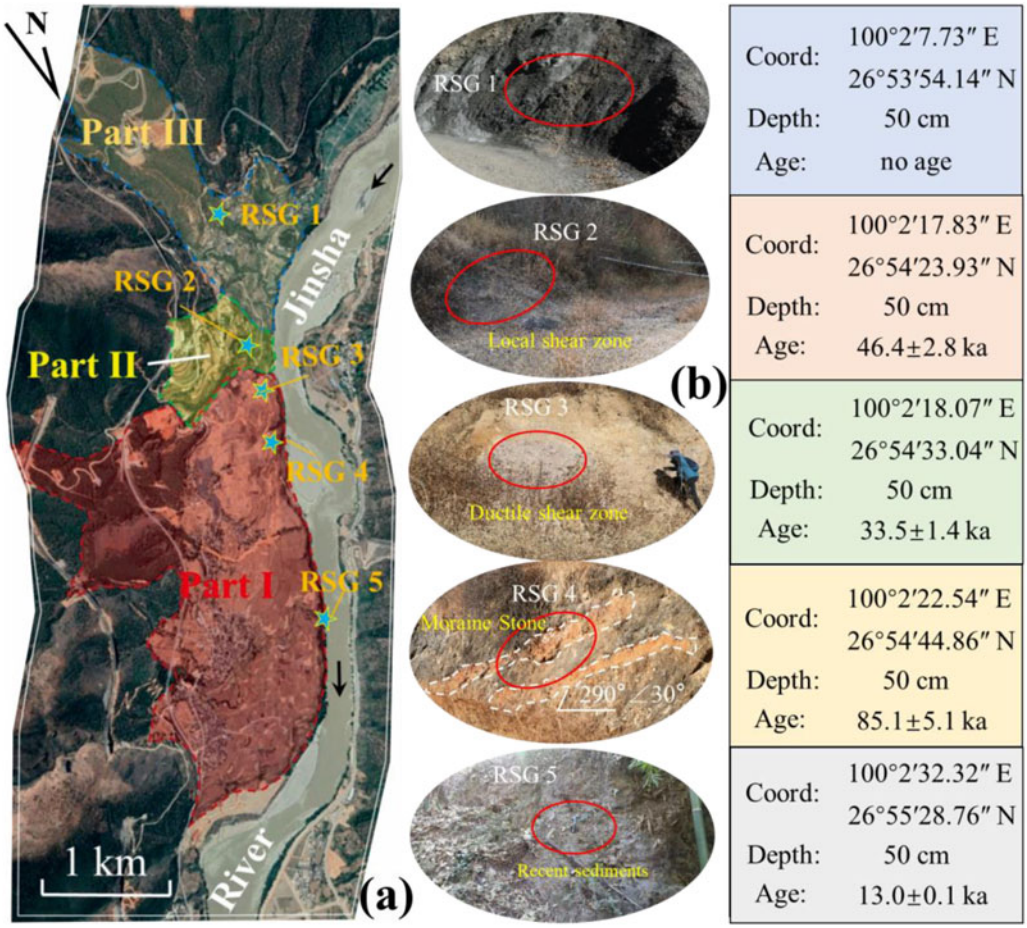

Figure 7. (a) Distribution of dated samples in parts I, II, and III. (b) Locations and ages of dated samples.

that can store energy in a stable radiation field is a constant. Therefore, the burial time (T) of deposits can be calculated according to the number of electrons accumulated (N) by mineral grains since burial time as a result of such radiation and the rate (B) at which the radiation has been received, namely T = N/B. Samples used for dating were collected from typical locations in different parts of the deposit (Fig. 7a). All deposits were sampled using stainless steel tubes on clean surfaces and sealed with aluminum foil to avoid exposure to light and moisture loss (Xu et al., 2015; W. Zhang et al., 2022). The samples were numbered RSG1–RSG5. Among them, RSG1 and RSG2 were collected from the local shear zone of Part III and Part II, respectively, representing the age of the debris-flow and the rock landslide (Fig. 7b). Three samples were collected from Part I due to its large scale (Fig. 7b). RSG3 came from the local ductile shear zone formed by the difference in velocity at the top of the deposit during movement of the moraine landslide, reflecting the time of the landslide (Part I). RSG4 came from the upper broken moraine rock block, reflecting the formation time of the moraine. RSG5 was collected from the riverbank of the front edge of Part I, which is a comparative sample of modern fluvial sediment.

All samples were used for fine particle component preparation under laboratory red light conditions (wavelength 640 ± 10 nm). Firstly, about 20 g were used to determine water content and the content of U, Th, and K. A central sample was then taken for screening (180 mesh). Organic matter and carbonates were removed using 40% hydrogen peroxide (H_2O_2) and 30% hydrochloric acid (HCl), respectively, after which 30% fluorosilicic acid ($H_2[SiF_6]$) was added. After five days, the sample was washed with distilled water until it reached a neutral pH. The suspension was placed in a beaker and allowed to stand to obtain 4–11 μm sized particles. The separated fine particle components were fully shaken and injected into the prepared funnel with stainless steel sheets. Finally, the experimental sample was obtained by drying fine-grained components precipitated in a funnel at a low temperature.

The test instruments used in this study were Daybreak 2000 Luminometer, 801E irradiator, and inductively coupled plasma mass spectrometry (ICP-MS). The sample equivalent dose and environmental dose were measured to eliminate errors. The equivalent dose was determined using a simple multi-aliquot regeneration method. After measuring the luminescent signals for both natural and regenerative doses, the samples were irradiated with an experimental dose, and the changes in sensitivity were monitored by measuring the luminescent signals corresponding to the experimental dose. The equivalent dose was then determined by calculating the ratio of the luminescence signal from the natural/regenerative dose to that of the subsequent experimental dose. The environmental dose was obtained by measuring the levels of radionuclides and water content, and it was further adjusted using the Fleming method (Fleming, 1971).

https://doi.org/10.1017/qua.2024.17 Published online by Cambridge University Press

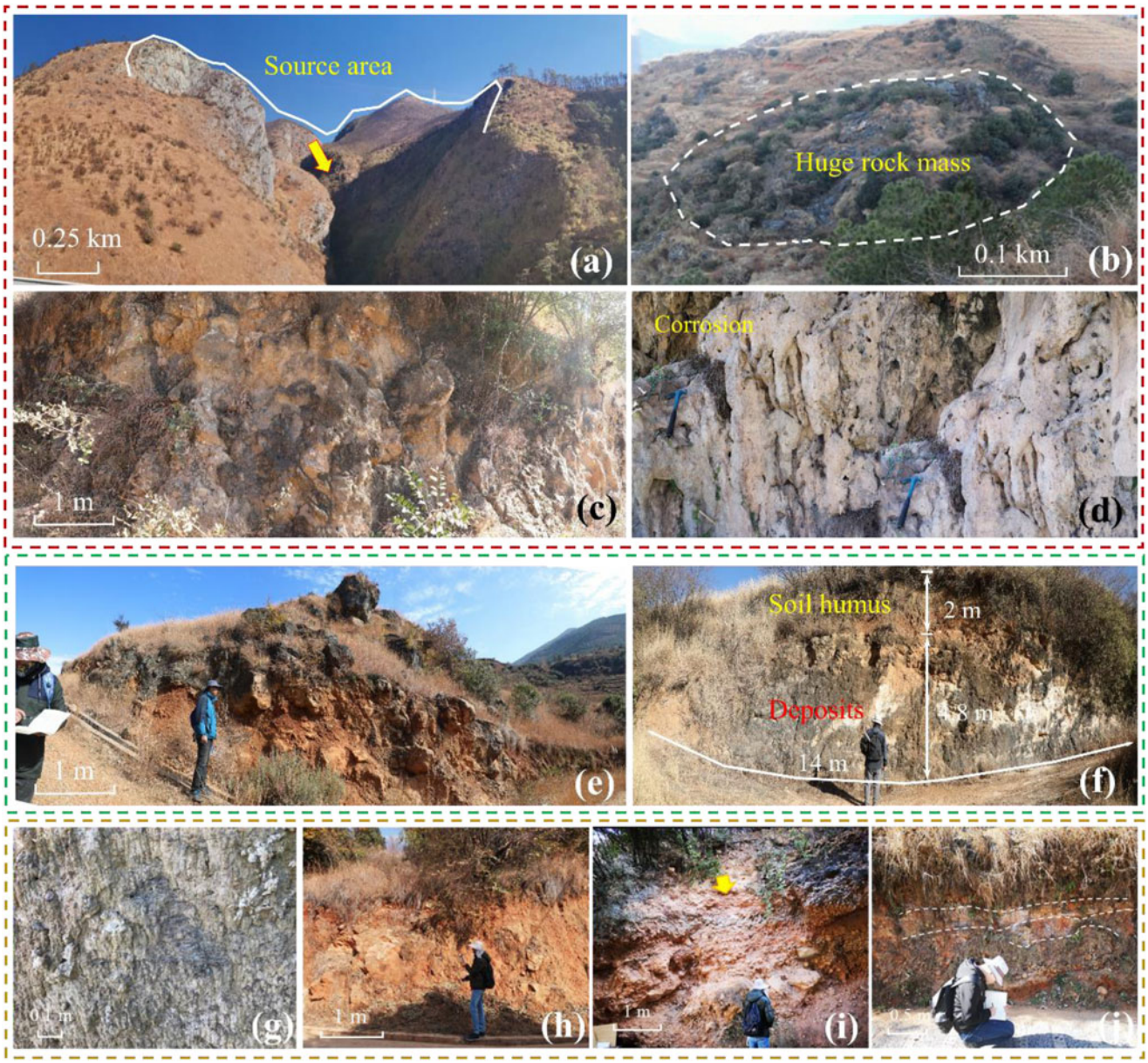

Figure 8. Field investigation of the HAD. (a) Source area of Part I; (b) huge rock mass embedded in Part I; (c) typical outcrop of Part I; (d) calcareous cementation and corrosion; (e) loose landslide deposits from Part II; (f) typical outcrop of Part II; (g) debris-flow deposits; (h) alluvial deposits; (i) material flow in debris-flow deposits; (j) stratification characteristics of debris flow deposits.

Results and Analysis

Geological characteristics of the deposit

Part I

Part I, the main part of the HAD, is a calcareous cement-rich deposit formed by a moraine landslide that has undergone extended physical and chemical alteration. There are mainly three judgment bases for moraine landslide: (1) the study area is significantly affected by Quaternary glaciation (Fig. 4b); (2) the cirque-shaped source area is characterized by typical early-glacial geomorphology and is a natural place for loose material storage (Fig. 8a); and (3) the sedimentological characteristics of the deposit are consistent with a moraine landslide. Several huge and complete rock masses (carbonate rocks) are embedded in the deposit (Fig. 8b), and some rock blocks are also scattered on the surface of the deposit. In addition, there are numerous unrounded, unsorted, and poorly graded rock blocks inside the deposit, which conforms to characteristics of moraine landslides (Fig. 8c). Part I has experienced a long evolution since its formation and is currently predominantly composed of calcareous cement. Affected by weathering and rainfall, these calcareous cements generally show significant signs of erosion (Fig. 8d).

Part II

Part II is a landslide deposit composed of loose and fully weathered carbonate rocks (Fig. 8e, f), whose lithology is consistent with that of the source area on its SE side (Fig. 6a). Because the strata of the source area are nearly upright with a trend that is nearly parallel to the Jinsha River, a high and steep slope structure

https://doi.org/10.1017/qua.2024.17 Published online by Cambridge University Press

has formed. Over time, geological forces acting on the rock mass have caused bending deformation and the formation of tensile cracks. Eventually, this deformation progressed to a toppling failure mode, resulting in the occurrence of the landslide. In terms of vertical sequence, Part I is situated above Part II, indicating that Part I was formed subsequent to the formation of Part II.

Part III

Part III consists of debris-flow (Fig. 8g) or alluvial deposits (Fig. 8h), which exhibit characteristics of material flow (Fig. 8i) and stratification (Fig. 8j). The presence of sorted and rounded gravel within the deposit serves as evidence that it has been transported by water flow. Situated at the starting point of the Yangbi valley, Part III showcases a prominent feature of the valley—its Quaternary sediment fill. Regarding vertical arrangement, Part II is positioned above Part III, indicating that the geomorphic pattern of the Yangbi valley and Part III was established prior to the formation of Part II.

Developmental characteristics of river sediments

The investigation of terraces from Shigu to HAD reveals the presence of three terraces (T_1, T_2, and T_3) in Shigu (Fig. 9a). Terraces T_2 and T_3 where the Shigu is located are 10–30 m higher than the

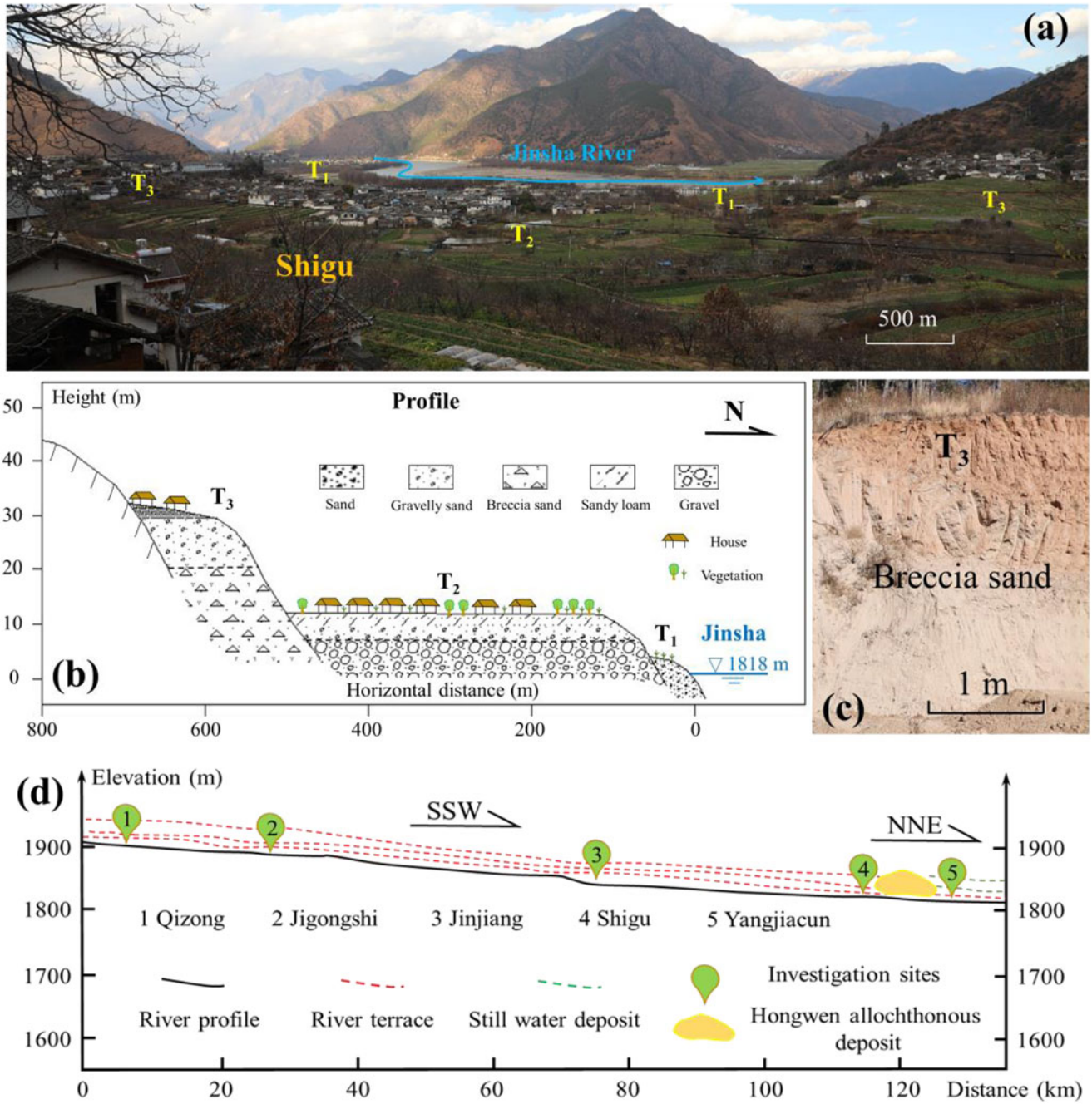

Figure 9. (a) Aerial view of the three terraces at Shigu. (b) Profile of the river terraces developed at Shigu (revised from Tong, 2019). (c) Typical outcrop of T_3. (d) Longitudinal profile of the First Bend reach showing river terraces (revised from Tong, 2019); arrows for SSW and NNE indicate the approximate flow direction of the river around the First Bend reach.

https://doi.org/10.1017/qua.2024.17 Published online by Cambridge University Press

river surface (Fig. 9b) and mainly composed of breccia sand or gravel sand (Fig. 9c). Terrace T_1 is less than 10 m higher than the river surface (Fig. 9b) and mainly composed of medium- to coarse-grained sand. Only one continuous terrace (T_1) is observed in the lower reaches of Shigu. Furthermore, river sediments were observed on the surface of the HAD. However, due to extensive artificial reconstruction, only certain portions of river sediments are exposed in the middle and upper sections of the deposit. This indicates that the ancient Jinsha River may have flowed through the middle and upper regions of the HAD in the past.

In a study conducted by Tong (2019) on river terraces, it was revealed that river sediments are well developed in the FBYR (Fig. 9d). The Qizong–Shigu section generally exhibits the presence of three terraces. However, the continuity of terrace development downstream of Shigu is relatively poor, which aligns with our existing understanding. By combining the river terrace profiles depicted by Tong (2019) for the Qizong–Shigu section with our investigation results on terrace distribution between Shigu and HAD, a comprehensive terrace profile of the FBYR has been established (Fig. 9d).

Chronology characteristics of the deposit and river sediments

Chronological measurements indicate that all samples, except for RSG1, exhibited normal luminescence signals and had corresponding equivalent dose values (Table 1). The dating results allowed us to establish that the moraine formed before 85 ka. The Part II and Part I deposits formed before 46.4 ± 2.8 ka and 33.5 ± 1.4 ka, respectively. Unfortunately, the age of Part III could not be determined directly due to insufficient luminescence signals. However, field investigation confirmed that the formation of Part III occurred earlier than that of Part II, indicating an earlier timeframe for the deposition of Part III.

The age estimation of river terraces is based on previous studies conducted by Tong (2019) (Table 2). Both Shigu and Qizong exhibit the presence of three terraces, while all corresponding terraces demonstrate comparable ages, with the exception of secondary terraces. Taking the Shigu area near the study site as an example, the ages of T_1, T_2, and T_3 are estimated to be 0.42 ka, 7.10 ka, and 10.53–14.18 ka, respectively. The vertical distance between two adjacent terraces ranges from 11–13 m.

Discussion

Paleoseismic events and paleoclimate characteristics

The chronological results obtained from the deposits necessitate analysis within the framework of paleostructural and paleoenvironmental evolution. Affected by the influence of tectonic movement and regional tectonic stress adjustment, an extremely rapid uplift phase began after the late Pleistocene (Fig. 3a) (Zhan et al., 2018; Li et al., 2020), which resulted in strong tectonic activities and several regional differential uplift events in the study area (Ming and Shi, 2006). Many faults have been reactivated by tectonic activities. The Longpan–Qiaohou fault exerts the most significant influence on the HAD. This fault is located along the posterior margin of the HAD, spanning approximately 120 km in length, and exhibiting an overall strike of 015–020°. Since the Late Quaternary, this fault has been characterized by strike-slip movement in mountainous regions and dip-slip movement in the basin areas. The maximum horizontal slip rate ranges from 3.10–6.45 mm/yr (Tang et al., 2014). The vertical slip rate has been estimated to be approximately 0.2 mm/yr to approximately 0.45 mm/yr since the late Pleistocene. According to the dating analysis of a paleoseismic trench in the Jianchuan basin, three seismic events have been identified along the Longpan–Qiaohou fault since the late Pleistocene (Tang et al., 2014). Notably, the timing of one paleo-earthquake event (33,860 ± 280 yr BP) (Tang et al., 2014; Li et al., 2022b) corresponds to the formation time (33.5 ka) for primary body (Part I) of the HAD.

The formation period of the HAD, ranging from 46.4–33.5 ka, represents a very interesting time node. Paleoclimate studies indicate that 40–30 ka falls within the interglacial epoch of the last glaciation in China (Shi et al., 1999), and it is the warmest period within the last glaciation (Shi et al., 2001). During this period, the most remarkable climatic characteristics were increasing temperatures, glacier retreat, and plentiful rainfall (Shi et al., 1999, 2001). This conclusion is drawn from various sources of evidence, such as the analysis of the Guliya ice core and examination of pollen records (Berger, 1978; Thompson et al., 1997; Shi et al., 2001; Xiao et al., 2013). These studies indicate that the temperature of the Tibetan Plateau was approximately 2–4°C higher than present-day temperatures, which has been attributed primarily to enhanced solar radiation during the summer season as a result of the precession cycle. High lake surface records from numerous large lakes in the Tibetan Plateau provide further evidence of abundant precipitation during that period, with rainfall levels estimated to be 1.4–2.0 times higher than the present (Shi et al., 2001). Prolonged rainfall and subsequent erosion and seepage have the potential to weaken the stability of rocks and soil in the source area. These climatic conditions create favorable circumstances for geological processes such as landslides or debris flows to occur.

Incision rate of the Jinsha River

The formation and evolution of the HAD cannot be discussed without considering the influence of river undercutting, the most direct manifestation of which is incision rate. River

Table 1. TL dating results.

Serial number	U (ppm)	Th (ppm)	K (%)	Equivalent dose (Gy)	Dose rate (Gy/ka)	water content	Age (ka)	Luminescent signal
RSG1	3.37	16.84	2.08	—	—	7.0 %	—	Less
RSG2	2.63	14.36	1.93	207.05 ± 9.7	4.46 ± 0.18	3.8 %	46.4 ± 2.8	Normal
RSG3	3.32	13.23	2.29	162.17 ± 2.7	4.85 ± 0.19	7.0 %	33.5 ± 1.4	Normal
RSG4	2.83	11.70	1.63	330.48 ± 15.0	3.88 ± 0.16	7.0 %	85.1 ± 5.1	Normal
RSG5	2.41	11.33	1.52	46.7 ± 3.5	3.59 ± 0.14	7.0%	13.0 ± 1.1	Normal

https://doi.org/10.1017/qua.2024.17 Published online by Cambridge University Press

Table 2. Age of river terraces at Qizong and Shigu (Tong, 2019).

Qizong			Shigu		
Terrace	Above the river (m)	Age (ka)	Terrace	Above the river (m)	Age (ka)
T_1	2	0.48 ± 0.08	T_1	5	0.42 ± 0.06
T_2	5	1.93 ± 0.24	T_2	16	7.10 ± 0.4
T_{31}	32	15.8 ± 1.01	T_{31}	28	10.53 ± 0.8
T_{32}	42	16.07 ± 0.91	T_{32}	29	14.18 ± 0.75

sediments exposed on the surface of the HAD can provide some insight into the incision rate of the Jinsha. Fluvial cobble–gravel was observed near the RSG3 sampling point during field work (Fig. 10a), indicating that the ancient Jinsha flowed through this area after the deposit formed. The river sediments exhibit good cementation characteristics but poor stratification. The distribution of cobble–gravel is discontinuous and is only visible in locally excavated outcrops. A reasonable explanation is that instability of the ancient Jinsha River during formation of the HAD, along with subsequent human activities, has made it exceptionally challenging to trace the deposition of river sediments. The only two outcrops available are roughly aligned with the elevation of RSG3. Therefore, the age of RSG3 (formation time of the HAD) can be assumed to be the same as that of the Jinsha sediments at the same elevation. RSG5 represents the age of modern river sediments. Combined with the elevation difference between RSG3 (1867 m) and RSG5 (1825 m), the incision rate of the Jinsha from 33.5–13 ka in the First Bend reach can be calculated as 2.05 mm/yr (Fig. 10b). To support this inference, it is necessary to gather chronological data and conduct incision-feature analysis derived from the study area's river terrace evolution. Table 2 shows that the terraces at Qizong and Shigu primarily represent three levels (T_1, T_2, and T_3) (Fig. 9d). The average incision rate of the river has greater significance over a longer time span. Therefore, taking the T_1 and T_3 terraces as a reference (Table 2), the average river incision rates of Shigu and Qizong are 2.566 mm/yr and 2.277 mm/yr, respectively. This result is similar to the incision rate inferred from the exposed river sediments on the surface of the HAD.

The average (2.3 mm/yr) of the incision rates mentioned above is adopted as the reference value for the incision rate in the study area. Considering the formation time of the main body of the HAD, it can be estimated that the river has experienced a downcutting depth of approximately 77 m since 33.5 ka. This value is similar to the thickness of the deposit, suggesting that the formation of the large-scale HAD may not have caused long-term blockage of the river. Furthermore, it indicates that the downcutting process of the river has been continuous rather than impeded by the deposition.

Genetic mechanism and geomorphological evolution of the HAD

The occurrence of mass movement events is typically influenced by various factors, especially the combined effects of heavy precipitation and seismic shaking (Dortch et al., 2009). Prolonged

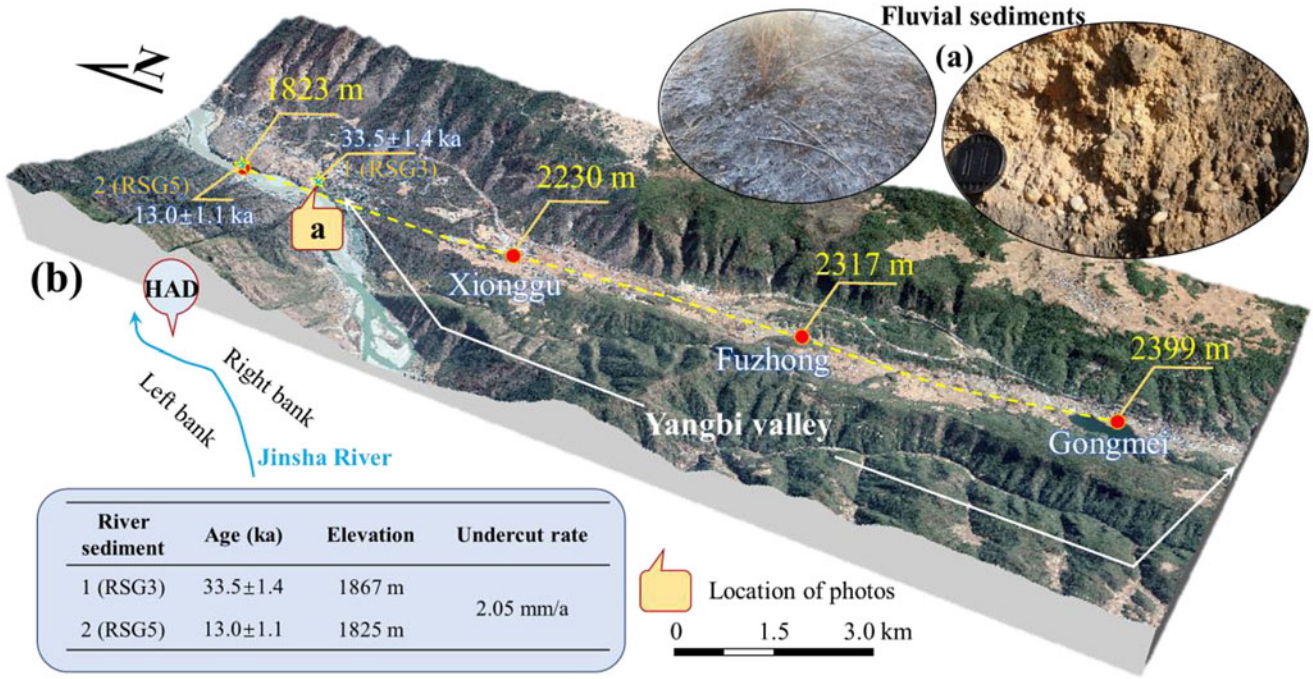

Figure 10. (a) River sediments exposed on the south side of the HAD. (b) Topographic characteristics of the Yangbi valley; inset table shows the incision rate of the Jinsha River, determined by examining the age and elevation of the river sediments exposed on the surface of the HAD (referenced from Li et al., 2022b).

https://doi.org/10.1017/qua.2024.17 Published online by Cambridge University Press

increases in precipitation can raise pore water pressure and reduce the strength of rock and soil, causing previously stable slopes to become unstable due to unloading, erosion, and tectonic activity. This process persists over the long term until the slope is pushed beyond its stability threshold (Owen et al., 2008). Simultaneously, intense precipitation also can lower the seismic acceleration required to trigger landslides. The paleoenvironmental analysis confirms that both tectonic activity and climate change indeed have significant effects on the formation of the HAD. Earthquakes, rainfall, snowmelt, and glacial processes may have all played important roles in the formation of the HAD. Therefore, it can be concluded that the HAD is a multi-source and multi-stage product of the synergistic effect of tectonic activity and climate change.

Based on field investigation, terrain interpretation, dating, and paleoenvironment analysis, an evolutionary sequence for the HAD has been proposed (Fig. 11), which indicates that 46.4 ka ago, a phase of the last glaciation was reaching its conclusion. With the tectonic activity and climate changes, the source areas of Part III and Part II underwent destruction and accumulated to the south of Hongwen. At 33.5 ka, a great interglacial stage of the last glaciation (the MIS 3 interstadial) began. This period held significant importance in the formation of gravity-driven deposits along the southeastern margin of the Qinghai–Tibet Plateau, as glaciers receded, temperatures increased, and rainfall significantly intensified.

Part I was formed by downslope movement of moraines, possibly triggered by some kind of geological force (earthquake, rainfall, rapid snowmelt, rapid glacial retreat, or a combination thereof), that had undergone erosion by rain and snowmelt over an extended period of time. Of course, the influence of river incision and downcutting cannot be ignored. Finally, a huge deposit (Part I) formed in the Jinsha River course. This deposit did not result in long-term river blockage, but it does not exclude the possibility of temporary channel obstruction. There are three observations supporting this judgment. (1) Lack of lacustrine deposits upstream of the deposit indicates that long-term river blockage did not occur. (2) The deposit front extends directly to the opposite bank, but no residual deposits are observed at the same elevation on the opposite bank. (3) The downcutting depth calculated based on incision rates since the deposit formation is similar to the thickness of the deposit itself. Although Part I did not cause a complete river blockage, its large scale still led to a temporary rise in river water level within a short

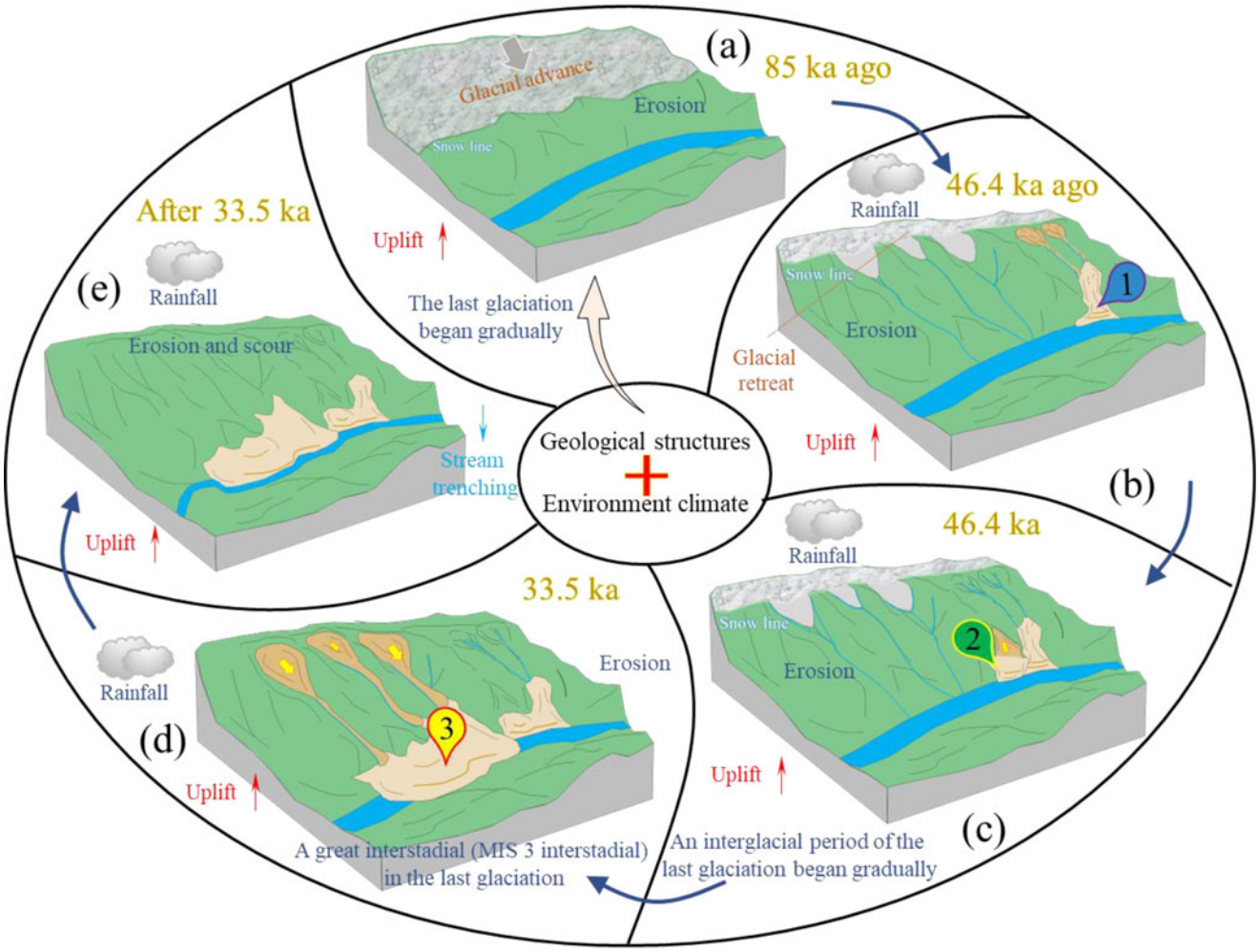

Figure 11. Schematic diagram of the formation and evolution of the HAD. (a) During the transition to the last glacial period, glacial advance gradually began and moraines were produced; (b) Part III was formed (since no effective dating data are available, the formation time in the figure is an estimate); (c) Part II was formed; (d) Part I was formed; (e) evolution of river landform after HAD formation. The numbers 1, 2, and 3 represent Part III, Part II, and Part I, respectively.

https://doi.org/10.1017/qua.2024.17 Published online by Cambridge University Press

period of time. With water level upstream rising gradually and eventually overtopping the front of the deposit, the leading edge was eroded. After formation of the new river course, the leading part of the deposit was rapidly carried downstream by high-energy water currents. Lateral erosion by these currents primarily affected the left bank, which was related to the topography of landslide deposit. The left bank was considerably eroded and scoured, resulting in almost no residual deposits, whereas the main body of the landslide remained relatively intact on the right bank. After that, with continuous downcutting of the river and supergene dynamic action, the current geomorphic features were formed.

The related analysis of the HAD can serve as a reference for studying the ancient deposits, recording both paleotectonic and paleoclimatic conditions. This contributes to a better understanding of the evolution of river systems in regions with complex geological conditions. As widely acknowledged, mass movement events, such as collapses, landslides, and debris flows, frequently occur in mountainous river valleys globally (Haque et al., 2019; Fan et al., 2020). In certain regions, these events often concentrate and exhibit a cascading effect (Zhan et al., 2018; Li et al., 2020). They are usually caused by complex geological environmental factors, such as tectonic activities, temperature fluctuations, rainfall patterns, glacial activity, and erosion and weathering processes (Shulmeister et al., 2009; Korup et al., 2012; Reznichenko et al., 2012; Kirschbaum et al., 2020; Lin et al., 2022; Zhao et al., 2023). The residual deposits accompany the subsequent processes of geomorphic evolution. Therefore, when investigating complex river geomorphic evolution issues, in addition to the geometric and sedimentological characteristics of the river system itself, dating analysis and the analysis of the genesis mechanism of ancient deposits can provide insights into paleoenvironments. This contributes to reconstructing geological history and enhancing the accuracy of the analytical results. In fact, researchers have already noted that the formation of extensive deposits often heralds extreme climate or tectonic events (W. Zhang et al., 2022). For example, in the Qinghai–Tibet Plateau and the surrounding mountain belts, the distribution frequency of ancient deposits over time often corresponds to periods of climate change and active tectonics (Li et al., 2023). Therefore, the unique geological historical period during which the HAD formed, as presented in this study, is likely just a microcosm of widespread mass movement on the Qinghai–Tibet Plateau. Future research on a larger spatial scale will contribute to reshaping this history, and the HAD can offer insights for related studies.

Conclusions

The formation of deposits plays a pivotal role in the evolutionary dynamics of a valley's geomorphology. In this study, we focused on investigating the allochthonous deposits and the river sediments of the First Bend of the Yangtze River (FBYR). Through analyzing the evolutionary process of the Hongwen allochthonous deposit (HAD) and the incision rate of the Jinsha River, we gained valuable insights into the paleostructure and paleoclimate characteristics of the region.

The HAD is a complex allochthonous deposit with diverse geological characteristics, resulting from a multi-source and multi-stage landslide influenced by the combined effects of tectonic activity and climate.

The HAD is categorized into three distinct parts, distinguished by their morphological and sedimentological features. Part I (3.52 km^2), the primary component of the HAD, is a calcareous cement-rich deposit resulting from a moraine landslide. Part II (0.53 km^2) consists of loose and fully weathered carbonate rocks forming a landslide deposit. Lastly, Part III (0.97 km^2) encompasses debris-flow or alluvial deposits characterized by material flow and stratification.

Following the late Pleistocene, a notable phase of rapid plateau uplift commenced, leading to intensified tectonic activity and several regional uplift events in the study area. The formation of the HAD took place between 46.4–33.5 ka, aligning with the significant interglacial stage of the last glacial period or the transitional period leading up to it. This timeframe was characterized by frequent tectonic activity, rising temperatures, increased rainfall, and heightened surface erosion.

The evolution of the HAD and the river sediments of the First Bend reach reveal that the average incision rate of the Jinsha over the past 33.5 thousand years was about 2.3 mm/yr.

The HAD represents the outcome of the combined influence of tectonic activity and climate change, serving as the primary mechanism driving surface processes in the First Bend region. The HAD has undergone a significant evolutionary process. Subsequently, with the continuous downcutting of the river and supergene dynamic action, the current geomorphic features were formed.

Acknowledgements. This work was supported by the National Natural Science Foundation of China (Grant No. 42307204, 41941017). The authors would like to thank the editor and anonymous reviewers for their comments and suggestions, which helped a lot in making this paper better.

Conflict of interest. The authors declare that they have no conflicts of interest related to this work.

Author contributions. Yuchao Li: conceptualization, methodology, investigation, writing-original draft; Jianping Chen: conceptualization and methodology; Qing Wang: resources, investigation, supervision, validation, review, and editing; Zhihai Li: investigation, data curation; Yansong Zhang: investigation, data curation; Jianhua Yan: language modification, investigation.

References

Allen, C.R., Gillespie, A.R., Yuan, H., Sieh, K.E., Buchun, Z., Chengnan, Z., 1984. Red River and associated faults, Yunnan Province, China: Quaternary geology, slip rates, and seismic hazard. *Geological Society of America Bulletin* **95**, 686–700.

Bao, Y., Zhai, S., Chen, J., Xu, P., Sun, X., Zhan, J., Zhang, W., Zhou, X., 2020. The evolution of the Samaoding paleolandslide river blocking event at the upstream reaches of the Jinsha River, Tibetan Plateau. *Geomorphology* **351**, 106970. https://doi.org/10.1016/j.geomorph.2019.106970.

Berger, A., 1978. Long-term variations of caloric insolation resulting from the Earth's orbital elements. *Quaternary Research* **9**, 139–167.

Burchfiel, B.C., Chen, Z., 2012. Tectonics of the southeastern Tibetan plateau and its adjacent foreland. *Geological Society of America Memoir* **210**, 231 pp.

Chen, J., Dai, F.C., Lv, T.Y., Cui, Z.J., 2013. Holocene landslide-dammed lake deposits in the Upper Jinsha River, SE Tibetan Plateau and their ages. *Quaternary International* **298**, 107–113.

Chen, J., Zhou, W., Cui, Z., Li, W., Wu, S., Ma, J., 2018. Formation process of a large paleolandslide-dammed lake at Xuelongnang in the upper Jinsha River, SE Tibetan Plateau: constraints from OSL and ^{14}C dating. *Landslides* **15**, 2399–2412.

Chung, S.L., Lee, T.Y., Lo, C.H., Wang, P.L., Chen, C.Y., Yem, N.T., Hoa, T.T., Genyao, W., 1997. Intraplate extension prior to continental extrusion along the Ailao Shan–Red River shear zone. *Geology* **25**, 311–314.

Costa, J.E., Schuster, R.L., 1988. The formation and failure of natural dams. *Geological Society of America Bulletin* **100**, 1054–1068.

https://doi.org/10.1017/qua.2024.17 Published online by Cambridge University Press

Cui, Z.J., Wu, Y.Q., Liu, G.N., Ge, D.K., Pang, Q.Q., Xu, Q.H., 1998. On Kunlun–Yellow River tectonic movement. *Science in China* (*Series D*) **41**, 592–600.

Dortch, J.M., Owen, L.A., Haneberg, W.C., Caffee, M.W., Dietsch, C., Kamp, U., 2009. Nature and timing of large landslides in the Himalaya and Transhimalaya of northern India. *Quaternary Science Reviews* **2**, 1037–1054.

Dunning, S.A., 2006. Formation and failure of the Tsatichhu landslide dam, Bhutan. *Landslides* **3**, 107–113.

EPICA community members, 2004. Eight glacial cycles from an Antarctic ice core. *Nature* **429**, 623–628.

Fan, X., Dufresne, A., Siva Subramanian, S., Strom, A., Hermanns, R., Tacconi Stefanelli, C., Hewitt, K., *et al.*, 2020. The formation and impact of landslide dams – state of the art. *Earth-Science Reviews* **203**, 103116. https://doi.org/10.1016/j.earscirev.2020.103116.

Fleming, S.J., 1971. Thermoluminescent dating principles and application. *Naturwissenschaften* **58**, 333–338.

Hao, M., Wang, Q.L., Shen, Z.K., Cui, D., Ji, L.Y., Li, Y.H., Qin, S.L., 2014. Present day crustal vertical movement inferred from precise leveling data in eastern margin of Tibetan Plateau. *Tectonophysics* **632**, 281–292.

Haque, U., da Silva, P.F., Devoli, G., Pilz, J., Zhao, B.X., Khaloua, A., Wilopo, W., *et al.*, 2019. The human cost of global warming: deadly landslides and their triggers (1995–2014). *Science of The Total Environment* **682**, 673–684.

Hermanns, R.L., Niedermann, S., Ivy-Ochs, S., Kubik, P.W., 2004. Rock avalanching into a landslide-dammed lake causing multiple dam failure in Las Conchas valley (NW Argentina) – evidence from surface exposure dating and stratigraphic analyses. *Landslides* **1**, 113–122.

Hungr, O., Leroueil, S., Picarelli, L., 2014. The Varnes classification of landslide types, an update. *Landslides* **11**, 167–194.

Kirschbaum, D., Kapnick, S.B., Stanley, T., Pascale, S., 2020. Changes in extreme precipitation and landslides over high mountain Asia. *Geophysical Research Letters* **47**, e2019GL085347. https://doi.org/10.1029/2019GL085347.

Kong, P., Na, C.G., Fink, D., Zhao, X.T., Xiao, W., 2009. Moraine dam related to late Quaternary glaciation in the Yulong Mountains, southwest China, and impacts on the Jinsha River. *Quaternary Science Reviews* **28**, 3224–3235.

Kong, P., Zheng, Y., Caffee, M.W., 2012. Provenance and time constraints on the formation of the first bend of the Yangtze River. *Geochemistry Geophysics Geosystems* **13**, Q06017. https://doi.org/10.1029/2012GC004140.

Korup, O., Clague, J.J., 2009. Natural hazards, extreme events, and mountain topography. *Quaternary Science Reviews* **28**, 977–990.

Korup, O., Montomery, D.R., 2008. Tibetan Plateau river incision inhibited by glacial stabilization of the Tsangpo Gorge. *Nature* **455**, 786–789.

Korup, O., Gorum, T., Hayakawa, Y., 2012. Without power? Landslide inventories in the face of climate change. *Earth Surface Processes and Landforms* **37**, 92–99.

Lai, Q.Y., Zhao, J.J., Huang, R.Q., Wang, D.J., Ju, N.P., Li, Q.M., Wang, Y.S., Xu, Q., Zhao, W.H., 2022. Formation mechanism and evolution process of the Chada rock avalanche in Southeast Tibet, China. *Landslides* **19**, 331–349.

Li, J.J., Fang, X.M., Ma, H.Z., Zhu, J.J., Pan, B.T., Chen, H.L., 1996. Geomorphological and environmental evolution in the upper reaches of the Yellow River during the late Cenozoic. *Science in China* (*Series D*) **39**, 380–390.

Li, J.J., Zhou, S.Z., Zhao, Z.J., Zhang, J., 2015. The Qingzang movement: the major uplift of the Qinghai–Tibetan Plateau. *Science China-Earth Sciences* **58**, 2113–2122.

Li, Y.C., Chen, J.P., Zhou, F.J., Song, S.Y., Zhang, Y.W., Gu, F.F., Cao, C., 2020. Identification of ancient river-blocking events and analysis of the mechanisms for the formation of landslide dams in the Suwalong section of the upper Jinsha River, SE Tibetan Plateau. *Geomorphology* **368**, 107351. https://doi.org/10.1016/j.geomorph.2020.107351.

Li, Y.C., Chen, J.P., Li, Z.H., Han, X.D., Zhai, S.J., Li, Y.C., Zhang, Y.W., Gu, F.F., 2022a. Comprehensive analysis of a paleo-landslide damming event on the upper reach of the Jinsha River, SE Tibetan Plateau. *Bulletin of Engineering Geology and the Environment* **81**, 334. https://doi.org/10.1007/s10064-022-02791-z.

Li, Y.C., Chen, J.P., Yan, J.H., Zhou, F.J., Wang, Q., Li, Z.H., Zhang, Y.S., 2022b. Formation and evolution of a giant old deposit in the First Bend of the Yangtze River on the southeastern margin of the Qinghai–Tibet Plateau. *Catena* **213**, 106138. https://doi.org/10.1016/j.catena.2022.106138.

Li, Y.C., Chen, J.P., Wang, Q., Chen, H.E., Bao, Y.D., Yan, J.H., Li, Z.H., 2023. Climate-driven formation of mass movements across the Tibetan Plateau. *Catena* **236**, 107721. https://doi.org/10.1016/j.catena.2023.107721.

Lin, Q.G., Steger, S., Pittore, M., Zhang, J.H., Wang, L.B., Jiang, T., Wang, Y., 2022. Evaluation of potential changes in landslide susceptibility and landslide occurrence frequency in China under climate change. *Science of The Total Environment* **850**, 158049. https://doi.org/10.1016/j.scitotenv.2022.158049.

Ming, Q.Z., Shi, Z.T., 2006. The forming factor analysis for the First Bend of Yangtse River. *IEEE International Symposium on Geoscience and Remote Sensing* **1–8**, 1587–1590. https://doi.org/10.1109/IGARSS.2006.409.

Owen, L.A., Kamp, U., Khattak, G.A., Harp, E., Keefer, D.K., Bauer, M.A., 2008. Landslides triggered by the 8 October 2005 Kashmir earthquake. *Geomorphology* **94**, 1–9.

Reznichenko, N.V., Davies, T.R.H., Shulmeister, J., Larsen, S.H., 2012. A new technique for identifying rock avalanche-sourced sediment in moraines and some paleoclimatic implications. *Geology* **40**, 319–322.

Searle, M.P., Yeh, M.W., Lin, T.H., Chung, S.L., 2010. Structural constraints on the timing of left-lateral shear along the Red River shear zone in the Ailao Shan and Diancang Shan Ranges, Yunnan, SW China. *Geosphere* **6**, 316–338.

Shi, Y.F., Liu, X.D., Li, B.Y., Yao, T.D., 1999. A very strong summer monsoon event during 30–40 ka BP in the Qinghai Xizang (Tibet) Plateau and its relation to precessional cycle. *Chinese Science Bulletin* **44**, 1851–1857.

Shi, Y.F., Yu, G., Liu, X.D., Li, B.Y., Yan, T.D., 2001. Reconstruction of the 40–30 ka BP enhanced India Monsoon climate based on geological records from the Tibetan Plateau. *Palaeogeography Palaeoclimatology Palaeoecology* **169**, 69–83.

Shulmeister, J., Davies, T.R., Evans, D.J.A., Hyatt, O.M., Tovar, D.S., 2009. Catastrophic landslides, glacier behaviour and moraine formation – a view from an active plate margin. *Quaternary Science Reviews* **28**, 1085–1096.

Strom, A.L., 2004. Rock avalanches of the Ardon River valley at the southern foot of the Rocky Range, Northern Caucasus, North Osetia. *Landslides* **1**, 237–241.

Tang, Y., Hu, C.Z., Tian, Q.J., Wang, L., Yang, P.X., Xiong, R.W., 2014. Preliminary study on paleo-earthquakes in Jianchuan section of Longpan–Qiaohou fault, Yunnan Province. *Earthquake* **34**, 117–124. [in Chinese]

Tapponnier, P., Peltzer, G., Armijo, R., 1986. On the mechanics of the collision between India and Asia. In: Coward, M.P., Ries, A.C. (Eds.), Collision Tectonics. *Geological Society of London, Special Publication* **19**, 113–157.

Thompson, L.G., Yao, T., Davis, M.E., 1997. Tropical climate instability the last glacial cycle from a Qinghai–Tibetan ice core. *Science* **276**, 1821–1825.

Tong, K.Y., 2019. Evolution characteristics of the landform of the first bay of the Yangtze River. Master's thesis, China University of Geosciences, Wuhan, China. [In Chinese with English abstract]

Trauth, M.H., Strecker, M.R., 1999. Formation of landslide-dammed lakes during a wet period between 40,000 and 25,000 yr B.P. in northwestern Argentina. *Palaeogeography, Palaeoclimatology, Palaeoecology* **153**, 277–287.

Wang, E., Burchfiel, B.C., 2000. Late Cenozoic to Holocene deformation in southeastern Sichuan and adjacent Yunnan, China, and its role in formation of the southeastern part of Tibetan Plateau. *Geological Society of America Bulletin* **112**, 413–423.

Wang, P.F., Chen, J., Dai, F.C., Long, W., Xu, C., 2014. Chronology of relict lake deposits around the Suwalong paleolandslide in the upper Jinsha River, SE Tibetan Plateau: implications to Holocene tectonic perturbations. *Geomorphology* **217**, 193–203.

Wei, H.H., Wang, E., Wu, G.L., Meng, K., 2016. No sedimentary records indicating southerly flow of the paleo-Upper Yangtze River from the First Bend in southeastern Tibet. *Gondwana Research* **32**, 93–104.

https://doi.org/10.1017/qua.2024.17 Published online by Cambridge University Press

Wu, Q.L., Zhao, Z.J., Liu, L., Granger, D.E., Wang, H., Cohen, D.J., Wu, X.H., *et al.*, 2016. Outburst flood at 1920 BCE supports historicity of China's Great Flood and the Xia Dynasty. *Science* **353**, 579–582

Xiao, D., Zhao, P., Wang, Y., Zhou, X., 2013. Modeling the climatic implications and indicative senses of the Guliya $\delta^{18}O$-temperature proxy record to the ocean–atmosphere system during the past 130 ka. *Climate of the Past* **9**, 735–747.

Xiao, X.C., Wang, J., 1998. A brief review of tectonic evolution and uplift of the Qinghai–Tibet Plateau. *Geological Review* **44**, 372–382.

Xu, H.Y., Jiang, H.C., Yu, S., Yang, H.L., and Chen, J., 2015. OSL and pollen concentrate ^{14}C dating of dammed lake sediments at Maoxian, east Tibet, and implications for two historical earthquakes in AD 638 and 952. *Quaternary International* **371**, 290–299.

Yan, J.H., Chen, J.P., Zhou, F.J., Li, Y.C., Zhang, Y.W., Gu, F.F., Zhang, Y.S., *et al.*, 2022. Numerical simulation of the Rongcharong paleolandslide river-blocking event: implication for the longevity of the landslide dam. *Landslides* **19**, 1339–1356.

Zhan, J.W., Chen, J.P., Zhang, W., Han, X.D., 2018. Mass movements along a rapidly uplifting river valley: an example from the upper Jinsha River, southeast margin of the Tibetan Plateau. *Environment Earth Science* **77**, 634. https://doi.org/10.1007/s12665-018-7825-4.

Zhang, D.F., Liu, F.Q., Bing, J.M., 2000. Eco-environmental effects of the Qinghai–Tibet Plateau uplift during the Quaternary in China. *Environmental Geology* **39**, 1352–1358.

Zhang, W., Wang, J., Chen, J., Soltanian, M. R., Dai, Z., WoldeGabriel, G., 2022. Mass-wasting-inferred dramatic variability of 130,000-year Indian summer monsoon intensity from deposits in the Southeast Tibetan Plateau. *Geophysical Research Letters* **49**, e2021GL097301. https://doi.org/10.1029/2021GL097301.

Zhang, Y.S., Chen, J.P., Zhou, F.J., Bao, Y.D., Yan, J.H., Zhang, Y.W., Li, Y.C., Gu, F.F., Wang, Q., 2022. Combined numerical investigation of the Gangda paleolandslide runout and associated dam breach flood propagation in the upper Jinsha River, SE Tibetan Plateau. *Landslides* **19**, 941–962.

Zhao, B., Su, L.J., Xu, Q., Li, W.L., Xu, C., Wang, Y.S., 2023. A review of recent earthquake-induced landslides on the Tibetan Plateau. *Earth-Science Reviews* **244**, 104534. https://doi.org/10.1016/j.earscirev.2023.104534.

Zhou, S.Z., Wang, X.L., Wang, J., Xu, L.B., 2006. A preliminary study on timing of the oldest Pleistocene glaciation in Qinghai–Tibetan Plateau. *Quaternary International* **154/155**, 44–51.

https://doi.org/10.1017/qua.2024.17 Published online by Cambridge University Press